The role of a mid-air collision in drifting snow

Shuming Jia[1,2], Zhengshi Wang[1,2],Shumin Li[1,2]

[1] State Key Laboratory of Aerodynamics, China Aerodynamic Research and Development Center, Mianyang Sichuan 621000, China

[2] Computational Aerodynamics Institute, China Aerodynamics Research and Development Center, Mianyang, Sichuan 621000, China

Correspondence: Zhengshi Wang (wangzs@cardc.cn)

Abstract. Drifting snow, a common two-phase flow movement in high and cold areas, contributes greatly to the mass and energy balance of glacier and ice sheets and further affects the global climate system. Mid-air collisions occur frequently in high-concentration snow flows; however, this mechanism is rarely considered in current models of drifting snow. In this work, a three-dimensional model of drifting snow with consideration of inter-particle collisions is established; this model enables the investigation of the role of a mid-air collision mechanism in openly drifting snow. It is found that the particle collision frequency increases with the particle concentration and friction velocity, and the blown snow with a mid-air collision effect produces more realistic transport fluxes since inter-particle collision can enhance the particle velocity under the same condition. However, the snow saltation mass flux basically shows a cubic dependency with friction velocity, which distinguishes it from the quadratic dependence of blown sand movement. Moreover, the snow saltation flux is found to be largely sensitive to the particle size distribution since the suspension snow may restrain the saltation movement. This research could improve our understanding of the role of the mid-air collision mechanism in natural drifting snow.

1 Introduction

As one of the most important indicators of global climate change, snow cover is widely distributed over high latitude regions (Mann et al., 2000;Gordon and Taylor, 2009;Huang and Shi, 2017). Drifting snow is an important natural phenomenon in which air flow carries snow particles traveling near the surface, which not only profoundly changes the mass and energy balance of polar ice sheets (Déry and Yau, 2002;Gallée et al., 2013;Huang et al., 2016) but also may induce various natural disasters, such as avalanches, landslides and mudslides (Christen et al., 2010;Schweizer et al., 2003;Sovilla et al., 2006). In-depth studies of the laws of snow particle motion and various influencing factors are essential for understanding this complex phenomenon.

Drifting snow in the turbulent boundary layer contains both saltation particles that jumps towards downwind at the near surface and suspension particles higher in the air. Inter-particle collision within aeolian snow/sand cloud changes trajectories of saltating grains, and further affects the structures and transportation features of the particle flow. Numerous of investigations have shown that mid-air collision effect plays an non-neglected role in wind-blown sand movement (Carneiro et al., 2013;Dong et al., 2005;Huang et al., 2007;Li et al., 2013). However, this mechanism has been rarely investigated in a drifting snow transport with more suspended grains and smaller particle response time.

Numerical simulations have become one of the most effective ways of exploring the blown snow movement, and plenty of drifting snow models have been established

since the end of last century. Generally, drifting snow models can be divided into Euler-Euler models (Bintanja, 2000;Déry and Yau, 1999;Lehning et al., 2008;Schneiderbauer and Prokop, 2011;Uematsu et al., 1991;Vionnet et al., 2013;Xiao et al., 2000) and Euler-Lagrange models (Huang et al., 2016;Huang and Shi, 2017;Huang and Wang, 2015, 2016;Nemoto and Nishimura, 2004;Zhang and Huang, 2008;Zwaaftink et al., 2014), in which snow particles are treated as one kind of continuous medium and individual particles, respectively. However, mid-air collisions, an important mechanism that influences the transportation of snow particles and the development of drifting snow, are hardly considered by current models. The Lagrange tracking model can capture the inter-particle collision process more explicitly and directly, and thus is more suitable for establishing the mid-air collision model.

In this work, a trajectory-based mid-air collision model for drifting snow is established on the basics of a three-dimensional drifting snow model in the turbulent boundary layer, and the effects of mid-air collision on the snow transportation and particle motion are mainly explored. This paper is structured as follows: Sect. 2 briefly introduces the model and method, Sect. 3 presents the model validation and simulation results, Sect. 4 discusses the results in detail, and Sect. 5 presents the conclusions.

2 Model and method

2.1 Turbulent boundary layer

The wind field is obtained from a large eddy simulation model of the Advanced

Regional Prediction System (ARPS, version 5.3.3) (Xue et al., 2001). Considering the coupling effect between the snow particles and air flow, the fluid governing equations can be written as (Dupont et al., 2013;Vinkovic et al., 2006):

$$\frac{\partial \rho}{\partial t} + \frac{\partial}{\partial x_i}(\rho \overline{u_i}) = 0 \tag{1}$$

$$\frac{\partial \rho u_i}{\partial t} + \frac{\partial \rho u_i u_j}{\partial x_j} = -\frac{\partial \tilde{p}^*}{\partial x_i} - \frac{\partial \tau_{ij}}{\partial x_j} + S_i \tag{2}$$

where ρ is the air density, t is time, x_i and u_i are the position coordinate and instantaneous wind velocity component, respectively, along three directions, $p^* = p' - \alpha\nabla(\rho\mathbf{u})$ includes the pressure perturbation and damping term (α is the damping coefficient), τ_{ij} is the sub-grid stress that is modeled by the Lagrangain dynamic closure model of Meneveau et al. (1996), and S_i is the source term that comes from the reaction force of the snow particles (Yamamoto et al., 2001):

$$S_i = -\frac{1}{\rho V_{grid}} \sum_{s=1}^{N_p} F_D \tag{3}$$

where V_{grid} and N_p are the volume and the number of particles in the grid cell, respectively. $F_D = m_p V_r f(Re_p)/T_p$ is the fluid drag force, where m_p is the mass of snow particle and V_r represents the relative speed between the snow particle and wind field, $T_p = \rho_p d_p^2 / 18\rho\nu$ is the particle relaxation time and represents the time of particle speed changing from one steady state to another, and ρ_p is the density of the snow particle. $Re_p = d_p V_r / \nu$ is the particle Reynolds number, where d_p is the particle diameter and ν is the kinematic viscosity of air. $f(Re_p)$ is a correction factor of particle drag coefficient and can be expressed as (Clift et al., 1978):

$$f(Re_p)=\begin{cases}1 & (Re_p<1)\\ 1+0.15\,\mathrm{Re}_p^{0.687} & (Re_p\geq 1)\end{cases} \tag{4}$$

2.2 Mid-air collision model

The Lagrange particle tracking method is used to calculate the trajectory of each snow particle. Considering the fluid drag force and gravity, the governing equation of particle motion can be read as (Anderson and Haff, 1988;Lopes et al., 2013):

$$\frac{dx_{pi}}{dt}=u_{pi} \tag{5}$$

$$\frac{du_{pi}}{dt}=F_{Di}+g_i(1-\frac{\rho}{\rho_p}) \tag{6}$$

where x_p and u_p are the position and velocity of snow particle, respectively, F_{Di} is the drag force component along the *i*-th direction, and g is the gravitational acceleration.

During the process of particle motion, the judgment criterion for a mid-air collision is $l<(d_A+d_B)/2$, in which $l=\sqrt{\sum(x_{Ai}-x_{Bi})^2}$ is the center distance of particle *A* and *B*. If particles *A* and *B* contact each other within a time step $(t, t+\Delta t)$, there must exists a root δt $(0<\delta t<\Delta t)$ that satisfies the following relation:

$$\frac{d_A+d_B}{2}=\sqrt{\sum((x_{Ai}-u_{Ai}\delta t)-(x_{Bi}-u_{Bi}\delta t))^2} \tag{7}$$

in which the smaller root will be used if two roots exist. Thus, the collision time of particles *A* and *B* is $t+\delta t$. Since mid-air particles judge collision event in sequence, each particle only seeks downstream particles to reduce computation.

To obtain particle information after the collision, the original coordinate system (X, Y, Z) is rotated to a new coordinate system (X_r, Y_r, Z_r), as shown in Fig. 1, in

which the X_r axis points from the center of particle A to that of B. In this condition, only the particle velocity component along the X_r axis is changed after the collision.

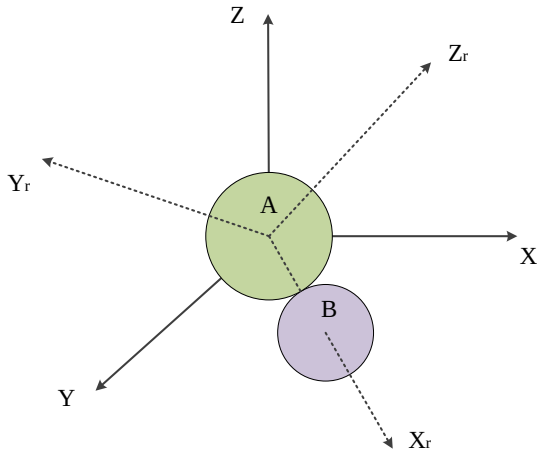

Figure 1. Schematic diagram of the rotation of the coordinate system.

Then, the particle velocity components ($\boldsymbol{u}_{Aci}$ and $\boldsymbol{u}_{Bci}$) in the new coordinate system can be calculated by the coordinate transformation algorithm. Since central collisions without particle rotation do not generate friction force, the particle velocity along the X_r axis after the collision in the new coordinate system can be expressed as:

$$\begin{cases} u'_{Ac1} = u_{Ac1} - \gamma d_B^3 (u_{Ac1} - u_{Bc1}) \\ u'_{Bc1} = u_{Bc1} + \gamma d_A^3 (u_{Ac1} - u_{Bc1}) \end{cases} \tag{8}$$

where $\gamma = (1+e) \Big/ \left(d_A^3 + d_B^3 \right)$ and e is the recovery coefficient of ice. According toHiga et al. (1998), the recovery coefficient of ice typically has a constant value e_{qe} at the quasi-elastic region and a decrement tendency at the inelastic region, which can be described by a piecewise function:

$$e = \begin{cases} e_{qe} & v_n < v_c \\ e_{qe} \left(\dfrac{v_n}{v_c} \right)^{-\log(v_n/v_c)} & v_n < v_c \end{cases} \tag{9}$$

in which $e_{qe} = 0.27\left(1+\hat{d}^3\right)^{0.1}\left(1+\hat{d}\right)^{0.2}\left(d_A/0.05\right)^{-0.5}$ and $\hat{d} \equiv d_A/d_B$, v_n is the

normal relative velocity of particle *A* and *B*, and v_c is the critical impact velocity for the transition from the quasi-elastic region to the inelastic region, which can be expressed as:

$$v_c = v_0\left(1+\hat{d}^3\right)^a\left(1+\hat{d}\right)^b \exp\left(\frac{c}{2RT}\right)\left(\frac{d_A}{d_0}\right)^{-0.5} \qquad T \geq 229K \tag{10}$$

where $v_0 = 5.72e-4$, $a = 3/4$, $b = -7/4$ and $d_0 = 0.03$ are parameters, R is the gas constant and T is the temperature.

Finally, the new coordinate system is rotated to the original location, and the particle velocity after the collision u'_{pi} can be obtained. The particle position after the collision can also be updated through $x'_{pi} = x_{pi} - u_{pi}\delta t + u'_{pi}\left(\Delta t - \delta t\right)$.

2.3 Simulation details

A computational domain of 2 m×1 m×1 m is adopted in this simulation. The grid number is 100×50×50, and grid stretch technology is used in the vertical direction (the finest grid scale is 2 mm). Under this grid resolution, the subgrid-scale (SGS) fluctuating velocity of particles has a negligible impact on particle motions, because the lifetime of SGS eddies is much smaller than the particle response time-scale (Dupont et al., 2013). The turbulence inflow boundary is used (Lund et al., 1998), and the outlet is an open radiation boundary condition. The periodic boundary conditions are adopted along the spanwise direction. The inlet flow obeys the logarithmic wind profile with a boundary layer depth of *H*=0.5 m and a roughness height of z_0 = 3.0×10^{-5} m (Nemoto and Nishimura, 2004, 2001). The bottom boundary is a rigid wall, and the top boundary obeys a stress-free boundary condition.

It is notable that the combined boundary conditions along streamwise are only

used to generate some initial wind fluctuations, and the periodic boundary conditions are adopted after that. The evolution time equals to 10 times of the large-eddy turnover time t_* ($t_* \equiv H/u_*$, where u_* is the friction velocity) under periodic boundary conditions. Drifting snow simulation begins after the turbulent boundary layer is fully developed, and the lateral boundary conditions for snow particles are the same as the wind field. Here, the friction velocity is obtained from the time and spatial averaged wind profile of a fully developed turbulent boundary layer without drifting snow according to the logarithmic law:

$$U(z) = \frac{u_*}{\kappa} \ln\left(\frac{z + z_0}{z_0}\right) \tag{11}$$

where $\kappa = 0.4$ is the Karman constant.

The aerodynamic entrainment scheme of (Zwaaftink et al., 2014) is used to induce a drifting snow in the turbulent boundary layer. In addition, the splash function for snow (Sugiura and Maeno, 2000) is used to describe the grain-bed interaction. Detailed formula for the aerodynamic entrainment and splash scheme can be seen in App. 1. Since the splash function is obtained from wind tunnel observations at low friction velocities, only the results at lower friction velocities (e.g., smaller than 0.5 ms^{-1}) are mainly discussed. Furthermore, the fracturing of the snow particle is not considered during particle collision, and the rotation of the particle is also neglected because the duration time of inter-particle collision is very short.

3 Results

3.1 Snow transport flux

The inter-particle collision within the drifting snow changes the trajectories of saltating particles, and further affect the structure and transport flux of the snow flow. Thus, the established drifting snow model is first verified by comparing the predicted snow transport flux with the measurements and other models.

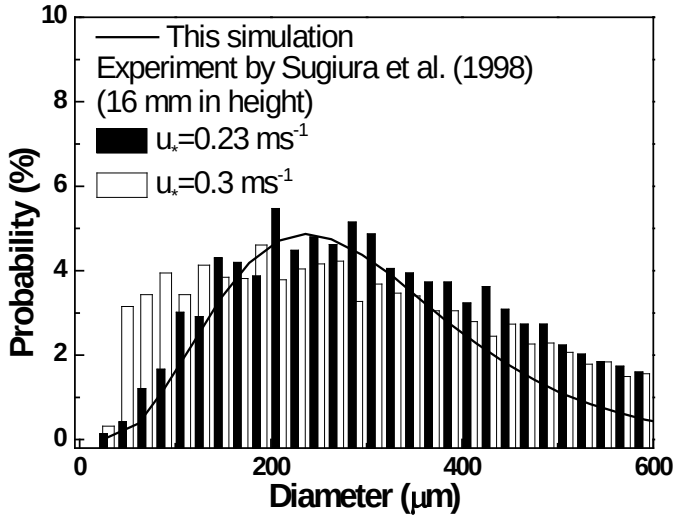

Figure 2. Particle size distribution in the simulation.

The particle size distribution of the snow sample is similar to that adopted by Nemoto and Nishimura (2004), as shown in Fig. 2, which follows the gamma function with a mean diameter of 250 μm. The gamma function can be written as:

$$P(d_p) = \frac{1}{\beta_p^{\alpha_p}\Gamma(\alpha_p)} d_p^{\alpha_p - 1} \exp(-\frac{d_p}{\beta_p}) \tag{12}$$

where $\alpha_p = 5$ and $\beta_p = 50$ are parameters. This distribution is also basically consistent with the experimental snow samples of Sugiura et al. (1998).

Before calculating the drifting snow process with mid-air collision, the validity of the collision model is examined firstly. Since the collision model judges collisions along the continuous particle trajectories within a particle integral time step, thus, the time resolution of the particle trajectory determines the accuracy of the model. Fig. 3

shows the predicted collision frequency versus particle concentration under various particle integral time steps Δt_p, which is also compared with theoretical results. Here, collision frequency is defined as the mean collision times per unit time of a particle.

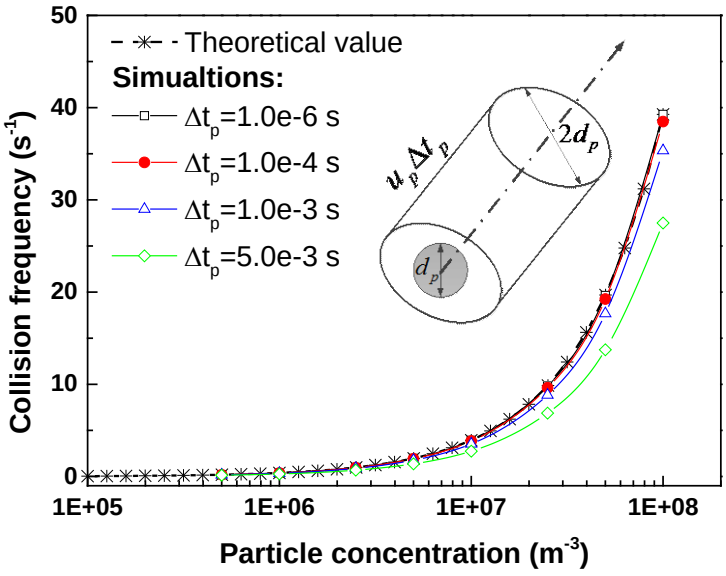

Figure 3. Comparison between theoretical collision frequency and simulation results under various particle integral time steps. The simulation condition is that a certain number of randomly released particles with uniform grain size moves in an airtight box (0.1 m×0.1 m×0.1 m). The initial velocity is 2.0 ms^{-1} with random directions, and the energy loss during inter-particle collision is neglected. The mirror reflection conditions without energy loss are adopted at boundaries. And the predicted collision frequency is the mean value of 10 s physical time. Besides, the theoretical collision frequency is calculated by the existence probability of particles in the control volume given by the inset ($\pi d_p^2 u_p \Delta t_p$). Thus, the theoretical collision frequency equals to $\pi d_p^2 u_p c$, where c is the number concentration of particles.

From Fig. 3, the predicted collision frequency is directly related to the particle integral time step, and the differences between various particle time steps increase

199 with particle concentration. A critical value of Δt_p =1.0e-4 s is necessary to capture
200 overall particle collisions. As a matter of fact, this critical value also ensures that most
201 particle displacement increments are smaller than the mean inter-particle gap (e.g., a
202 particle concentration of 1.25×10^{8} m^{-3} corresponding a mean inter-particle gap of
203 1.75×10^{-3} m). However, a larger time step for particle may miss part of collisions,
204 because the displacement increments of particle are larger than the mean inter-particle
205 distance. In this simulation, the selected time step ensures that the error between
206 simulation and theoretical results under extreme condition (maximum particle
207 concentration and particle velocity) is smaller than 5%.

208 Snow transport fluxes with and without a mid-air collision mechanism are shown
209 in Fig. 4. From this figure, it can be seen that without mid-air collisions, the snow
210 transport flux at various friction velocities are consistent with the simulation results of
211 Nemoto and Nishimura (2004), mainly because the same splash function is adopted.

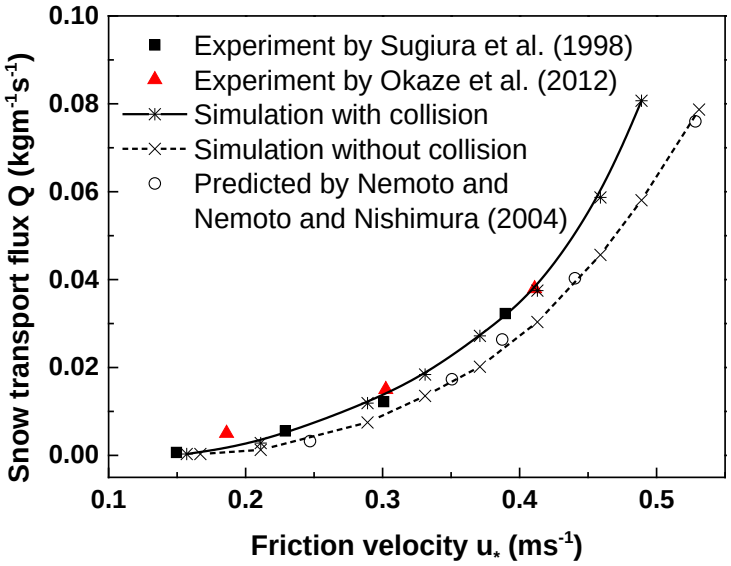

212

213 **Figure 4.** Snow transport flux versus friction velocity.

214 However, the snow transport flux is obviously enhanced with inter-particle

collisions than without mid-air collisions, and the snow transport flux with mid-air collisions is obviously closer to the measurements (Okaze et al., 2012;Sugiura et al., 1998), which indicates that mid-air collisions are not negligible within drifting snow. At the same time, the enhanced proportion increases with increasing friction velocity. For example, at approximately the critical friction velocity (the smallest friction velocity for a drifting snow), the snow transport flux with and without mid-air collisions is almost equal. However, when the friction velocity reaches 0.489 ms^{-1}, the enhanced proportion by mid-air collisions is up to 38.97%. The reason could be that frequent collisions between higher and lower particles in the snow flow, on the one hand, increase the momentum of the impacting particles, and on the other hand, send the falling particles back to high altitude to obtain more energy. At the same time, saltating particles reduce the wind at the near surface, however, mid-air collisions reduce the surface wind speed to a more smaller value, which also implies that the mass flux is enhanced by mid-air collision effect, detailed discussion can be seen in Sec. 4.2.

3.2 Collision frequency

The collision frequency under various friction velocities is shown in Fig. 5. Here, the collision frequency is defined as the collision times per unit time of a saltating particle. It can be seen that the collision frequency is directly related to the particle concentration. When the particle concentration is below 1.0e6 m^{-3}, inter-particle collisions rarely occur. However, with the further increment in the particle concentration, the frequency of the inter-particle collision event increases rapidly, and

one particle may experience over 10 collisions per second when the particle concentration is 1.0×10^{8} m^{-3}.

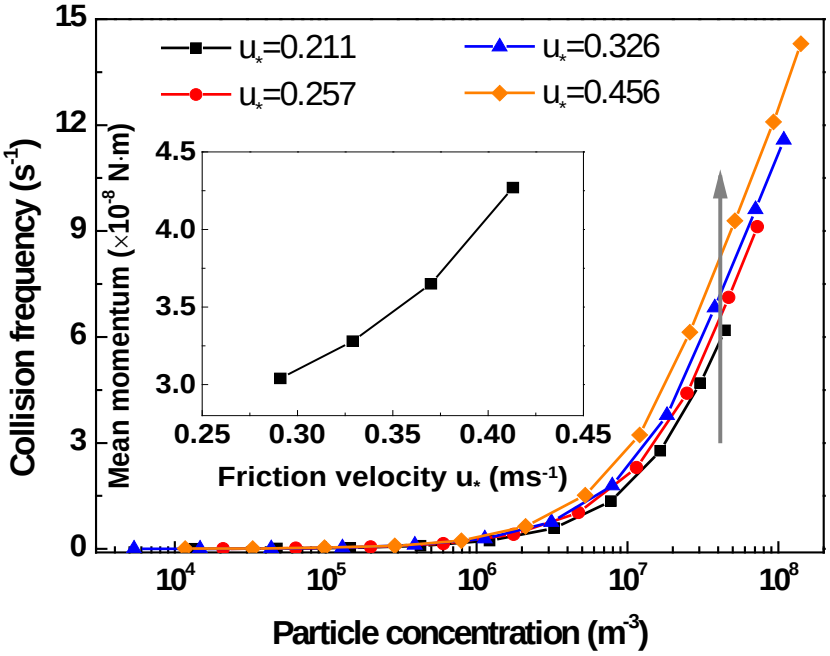

Figure 5. Inter-particle collision frequency versus particle concentration under various friction velocities (inset: mean particle momentum of saltating snow particle in drifting snow).

In addition, the collision frequency also increases with the friction velocity at the same particle concentration. The reason could be that the mean particle momentum increases with friction velocity, and as shown in the inset, the mean particle momentum tends to increase with friction velocity, which is also consistent with the experimental measurements (Nishimura et al., 2015;Nishimura and Hunt, 2000).

As a matter of fact, the particle volume fraction of snow cloud reflects the gaps among solid particles, and determines the collision frequency more directly. Elghobashi [1994] reported that the inter-particle collision effect is not negligible when the particle volume fraction exceeds 10^-3, which corresponds to a particle

concentration of $\sim 10^8$ m^{-3} in our simulation. For a drifting snow process, only the near surface transport particle cloud achieves this condition, and our simulation results also show that the structures of near surface snow cloud are largely reshaped by mid-air collisions. From Fig. 5, it can be seen that the collision frequency is about 10 per second, which implies that almost each saltation process is affected by mid-air collisions (the time scale of a saltation process is approximately 0.1s).

From the above analysis, drifting snow generally exists at a critical height, i.e., mid-air collisions frequently occur below this height, while there are few collision events above this height. As shown in Fig. 6, the critical height h_c basically increases linearly with the friction velocity when the critical particle concentration of 1.0e6 m^{-3} is adopted, and the function of $h_c = 1.42 + 20.8u_*$ properly describes the tendency.

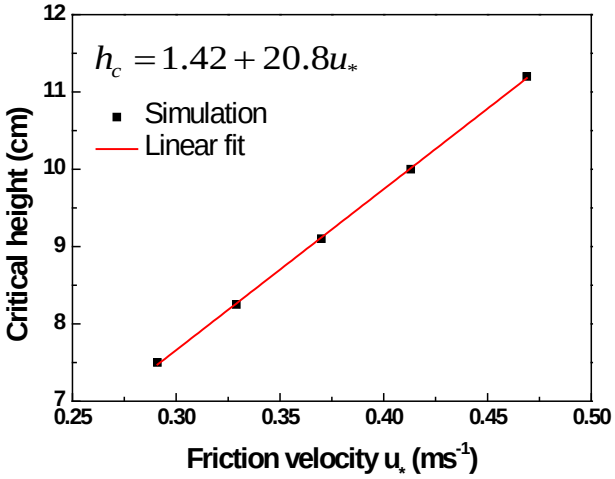

Figure 6. Critical height for the mid-air collision in drifting snow.

4 Discussions

4.1 Effect of mid-air collision on the structure of drifting snow

Mid-air collision changes trajectories of saltating grains, and further affects the

structure of transport snow cloud. Fig. 7 shows snow transport flux profiles with and without mid-air collisions. Generally, drifting snow models without mid-air collision always tends to overestimate the mass flux at the near surface, as shown in Fig. 7 and predictions by Nemoto and Nishimura (2004). However, with the mid-air collision effect into consideration, it can be seen that the mass flux at the near surface is largely reduced, while the snow transport flux higher in the air is largely enhanced, and the modified transport flux profile is closer to the tendency of observations. The main reason could be that numbers of particles are extruded out from the high concentration snow cloud at the near surface by frequent mid-air collisions.

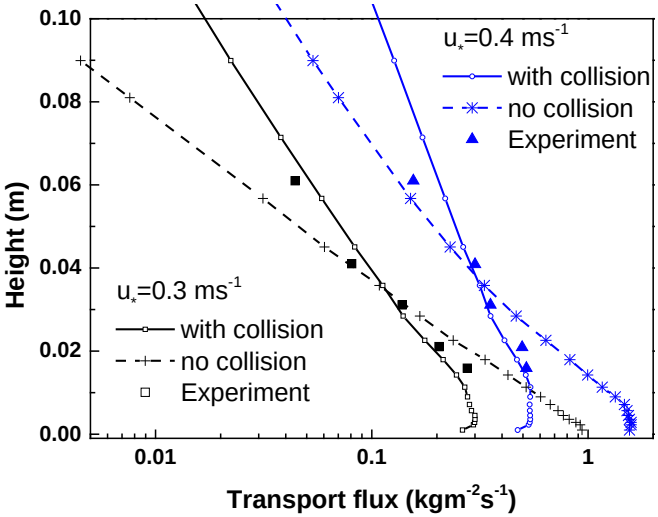

Figure 7. Mass flux profiles with and without mid-air collisions.

Since mid-air collisions plays an important role in conveying particles to high altitude, the enhanced total transport flux under mid-air collision should be mainly contributed by the increased transport flux higher in the air. This is substantially accord with the findings of Carneiro et al. (2013). In this way, the particle concentration profile is also modified by mid-air collisions. As shown in Fig. 8, part of the near surface particles are transported to higher altitude by inter-particle

collision, and the particle concentration profiles is largely changed by mid-air collision effect. The inset shows the particle concentration profile at the near surface.

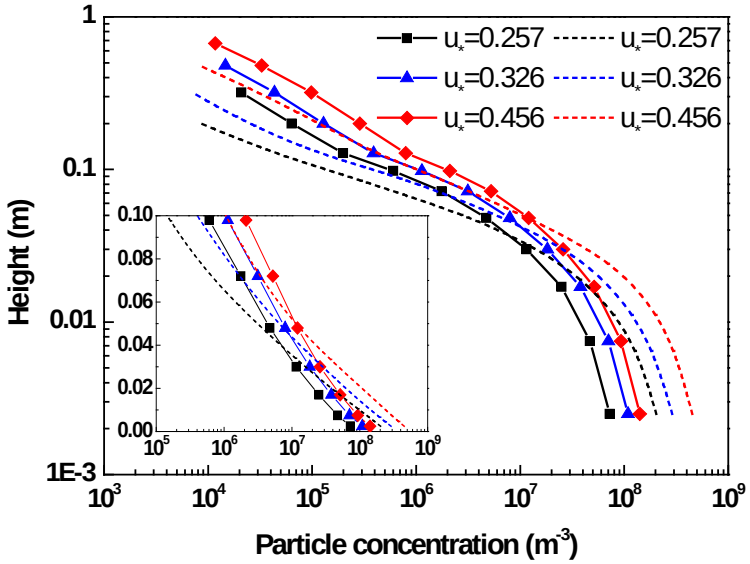

Figure 8. Profiles of particle number concentration with and without mid-air collisions under various friction velocities (Solid lines: with mid-air collisions; dashed lines: without mid-air collisions).

Seen from Fig. 8, the thickness of the drifting snow layer is increased by mid-air collision effect under the same friction velocity, which is also a positive contribution to the increment of the total mass flux. Mid-air collisions also increase the particle concentration higher in the air but reduce that at the near surface, agree well with the mass flux profiles.

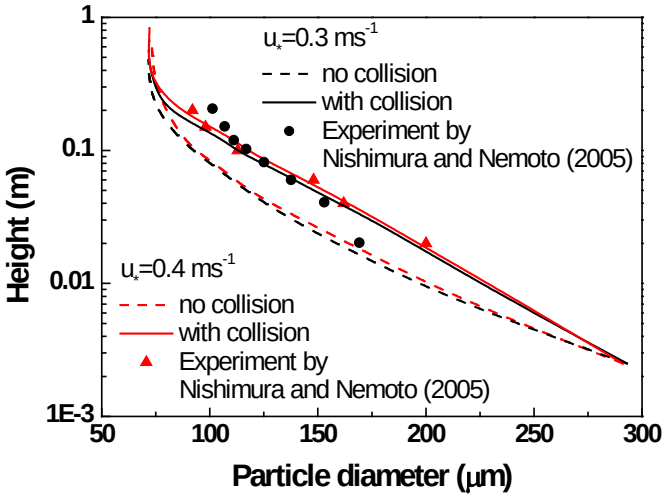

297

298 **Figure 9.** Profiles of particle mean diameter under various friction velocities.

299 At the same time, the thickness of the drifting snow layer with atmospheric
300 turbulence is much larger than that without turbulence, which also increases with
301 friction velocity. The reason could be that turbulent vortex brings particles to higher in
302 the air when the local vertical wind speed exceeds the particle's terminal velocity, and
303 turbulent intensity also increases with friction velocity. Generally, smaller particles
304 are easier to be transported to higher altitude, thus, the mean particle diameter
305 decreases with height, as shown in Fig. 9. However, with mid-air collision effect into
306 consideration, more larger snow particles are transported to higher in the air, thus, the
307 mean particle diameter at higher altitude becomes larger. This tendency is closer to
308 the observations by Nemoto and Nishimura (2005).

309 4.2 Surface shear stress with and without collision

310 In steady-state drifting snow, part of the downward horizontal momentum flux in the
311 saltation layer is carried by saltating snow particles, and thus the total downward
312 momentum flux τ equals the sum of the horizontal momentum fluxes due to particles
313 τ_p and the fluid τ_f, that is, $\tau = \tau_p + \tau_f$ (Kok et al., 2012;Raupach, 1991). The

residual fluid shear stress τ_f, also called the impact threshold, represents the threshold of the fluid shear stress that retains the particle splash process and is commonly treated as a constant in the steady-state saltation (Bagnold, 1941;Owen, 1964).

However, several recent physically based numerical saltation models and measurements indicate that τ_f in fact decreases with the friction velocity mainly because the larger wind speed higher in the saltation layer should be compensated by a decrease in the wind speed lower in the saltation layer (Kok et al., 2012;Walter et al., 2015). This is also true for drifting snow, as shown in Fig. 6(a). In this simulation, coarse snow particles are adopted since pure saltation with least suspended snow is wanted, the particle size distribution is shown in Fig. 6(b). It can be seen that the particle size is larger than 100 μm because the diameter of the suspension snow is basically smaller than 100 μm (Gordon and Taylor, 2009;Huang and Wang, 2015;Nemoto and Nishimura, 2004;Nishimura and Hunt, 2000).

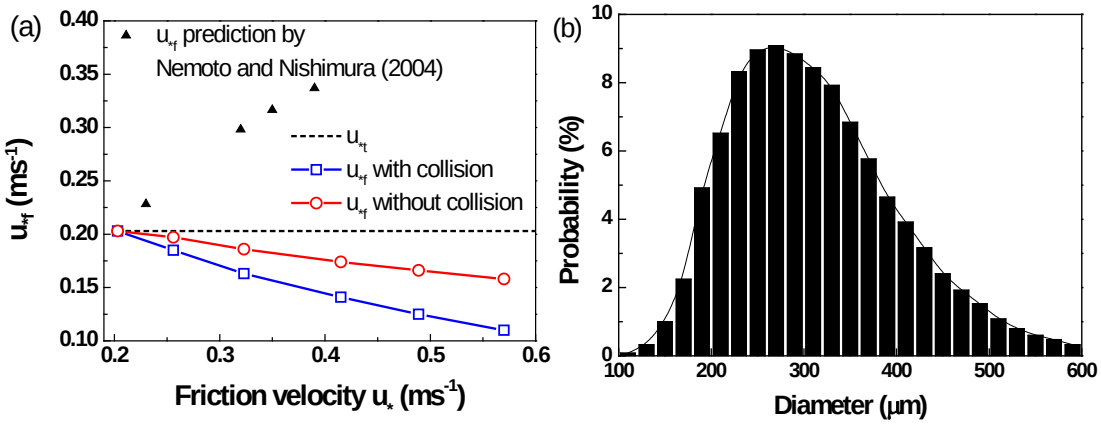

Figure 6. (a) Variation in the fluid stress versus friction velocity, and (b) particle size distribution for the pure saltation simulation.

Additionally, the presence of mid-air collisions further decreases the impact

threshold to a great extent. As shown in Fig. 6(a), under the same friction velocity condition, the residual fluid shear stress τ_f with the mid-air collision effect is smaller than that without mid-air collisions, mainly because frequent inter-particle collisions convey part of particles to higher in the air where the wind speed is larger, the overall particle energy and thus the saltation is enhanced.

It is known that the saltation mass flux can be derived from the momentum balance in the saltation layer as(Kok et al., 2012;Sørensen, 2004):

$$Q = \rho\left(u_*^2 - u_{*f}^2\right) L / \Delta\overline{V} \tag{13}$$

where u_{*f} is the critical impact friction velocity, L is the mean saltation length, and $\Delta\overline{V}$ is the mean velocity difference of the impact and lift-off particles. Many numerical and experimental investigations present the scaling of the saltation mass flux Q with u_*^3 (Bagnold, 1941;Clifton et al., 2006;Nishimura and Hunt, 2000;Owen, 1964;Vionnet et al., 2013) by assuming that the particle speeds can be linearly scaled with the friction velocity u_*, and u_{*f} is commonly approximate with the critical fluid friction velocity $u_{*\mathrm{t}}$. Whereas the critical impact friction velocity u_{*f} may be larger or smaller than the critical fluid friction velocity $u_{*\mathrm{t}}$ as a matter of fact, as shown in Fig. 6(a).

For wind-blown sand movement, recent studies have proved that the saltation mass flux actually shows a quadratic dependency with the friction velocity since the mean particle speed in the saltation layer is independent of the friction velocity (Durán et al., 2011;Ho et al., 2011;Kok et al., 2012). For drifting snow, however, the mean particle speed at the near surface is essentially proportional to the friction

velocity (Nishimura and Hunt, 2000;Nishimura et al., 2015) probably due to the smaller response time of the snow particle, which supports the fact that the snow saltation flux typically shows a cubic dependency.

Interestingly, Nemoto and Nishimura (2004) reported an increasing tendency of the fluid stress τ_f with the friction velocity when suspension snow is included, as shown in Fig. 6(a). This increase may be because suspended snow reduces the wind speed higher in the air, which in turn need a larger wind speed lower in the saltation layer to replenish the particle momentum. Thus, the suspension snow may restrain the saltation movement. The measurements of Nishimura and Hunt (2000) with various snow grain sizes also support this point.

In this way, the saltation mass flux (or residual fluid stress) of drifting snow largely depends on the particle size. For pure saltation movement as in above simulation (e.g., coarse grain size), τ_f decreases with the friction velocity and results in a larger saltation flux. Whereas for drifting snow with considerable suspended snow particles, τ_f may increase with friction velocity, and thus reduce the saltation mass flux. That is, snow samples with different grain sizes may have different saltation mass fluxes under the same wind condition. The particle borne stress τ_p from the above simulation is approximately 4.5 times that predicted by the model of Nemoto and Nishimura (2004) when the friction velocity is 0.39 ms^{-1}, and thus, the snow saltation flux may be considerably different.

As a matter of fact, measurements of Sugiura et al. (1998) have shown that the total mass flux (including saltation and suspension) is rather sensitive to the particle

size, because the suspension mass flux varies significantly. From this study, the suspension and saltation snows also influence each other. Most previous drifting snow models adopted by the mass balance studies of glaciers of ice caps consider the saltation and suspension processes independently (Gallée et al., 2001;Lehning et al., 2008;Vionnet et al., 2013). From above analysis, this may increase the uncertainty of prediction with varying grain sizes. A coupling model that includes the interactions between saltation and suspension snows is necessary to model the drifting snow process more exactly.

5 Conclusions

In this work, a three-dimensional drifting snow model in the turbulent boundary layer with consideration of a mid-air collision mechanism is established based on tracking the trajectory of each snow particle; this model enables the exploration of the mid-air collision mechanism on the drifting snow process exactly.

In the traveling snow flow, mid-air collisions play an important role in enhancing the snow transport flux. The enhanced total transport flux is mainly contributed by the increased mass flux higher in the air, since mid-air collisions change the structure of drifting snow layer by reducing the mass flux at the near surface but increasing that higher in the air. In addition, there exists a critical particle concentration in which inter-particle collisions rarely occur below this value. However, above the critical concentration, the collision frequency as well as the role of inter-particle collisions is found to increase with the friction velocity.

Furthermore, mid-air collisions also enhances the particle velocity by conveying

more particles to higher in the air, and thus further reduces the residual fluid stress during drifting snow conditions. The snow saltation flux is also found to be sensitive to particle size distribution of the snow samples because suspension snow may restrain saltation movement to a great extent, and the snow saltation flux may vary several times for different particle size distribution.

Acknowledgements

This work is supported by National key research and development program (2016YFC0500901), Forestry industry research special funds for key public welfare projects (201404306), National Natural Science Foundation of China (11772143) and 111 Project, B14044, CARDC Fundamental and Frontier Technology Research Fund (FFTRF-2017-08, FFTRF-2017-09).

References

Anderson, R. S., and Haff, P. K.: Simulation of Eolian Saltation, Science, 241, 820-823, 1988.

Anderson, R. S., and Haff, P. K.: Wind modification and bed response during saltation of sand in air, Acta. Mech., 1, 21-51, 1991.

Bagnold, R. A.: The Physics of Wind Blown Sand and Desert Dunes, Methuen, London, 1941.

Bintanja, R.: Snowdrift suspension and atmospheric turbulence. Part I: Theoretical background and model description, Boundary-Layer Meteorology, 95, 343-368, 2000.

Carneiro, M. V., Araújo, N. A., Pähtz, T., and Herrmann, H. J.: Midair collisions enhance saltation, Phys.rev.lett, 111, 058001, 2013.

Christen, M., Kowalski, J., and Bartelt, P.: RAMMS: Numerical simulation of dense snow avalanches in three-dimensional terrain, Cold Regions Science & Technology, 63, 1-14, 2010.

Clift, R., Grace, J. R., and Weber, M. E.: Bubbles, drops, and particles, Academic Press, 263-264 pp., 1978.

Clifton, A., Rüedi, J. D., and Lehning, M.: Snow saltation threshold measurements in a drifting-snow wind tunnel, Journal of Glaciology, 52, 585-596, 2006.

Déry, S. J., and Yau, M. K.: A Bulk Blowing Snow Model, Boundary-Layer Meteorology, 93, 237-251, 1999.

Déry, S. J., and Yau, M. K.: Large‐scale mass balance effects of blowing snow and surface sublimation, Journal of Geophysical Research Atmospheres, 107, 8-17, 2002.

Dong, Z., Huang, N., and Liu, X.: Simulation of the probability of midair interparticle collisions in an aeolian saltating cloud, Journal of Geophysical Research Atmospheres, 110, 2005.

Doorschot, J. J. J., and Lehning, M.: Equilibrium Saltation: Mass Fluxes, Aerodynamic Entrainment, and Dependence on Grain Properties, Boundary-Layer Meteorology, 104, 111-130, 2002.

Dupont, S., Bergametti, G., Marticorena, B., and Simoëns, S.: Modeling saltation intermittency, Journal of Geophysical Research Atmospheres, 118, 7109-7128, 2013.

Durán, O., Claudin, P., and Andreotti, B.: On aeolian transport: Grain-scale interactions, dynamical mechanisms and scaling laws, Aeolian Research, 3, 243-270, https://doi.org/10.1016/j.aeolia.2011.07.006, 2011.

Gallée, H., Guyomarc'H, G., and Brun, E.: Impact Of Snow Drift On The Antarctic Ice Sheet Surface Mass Balance: Possible Sensitivity To Snow-Surface Properties, Boundary-Layer Meteorology, 99, 1-19, 2001.

Gallée, H., Trouvilliez, A., Agosta, C., Genthon, C., Favier, V., and Naaim-Bouvet, F.: Transport of Snow by the Wind: A Comparison Between Observations in Adélie Land, Antarctica, and Simulations Made with the Regional Climate Model MAR, Boundary-Layer Meteorology, 146, 133-147, 2013.

Gordon, M., and Taylor, P. A.: Measurements of blowing snow, Part I: Particle shape, size distribution, velocity, and number flux at Churchill, Manitoba, Canada, Cold Regions Science & Technology, 55, 63-74, 2009.

Higa, M., Arakawa, M., and Maeno, N.: Size Dependence of Restitution Coefficients of Ice in Relation to Collision Strength, Icarus, 133, 310-320, 1998.

Ho, T. D., Valance, A., Dupont, P., and Ould, E. M. A.: Scaling laws in aeolian sand transport, 2011, 1059-1062.

Huang, N., Zhang, Y., and D'Adamo, R.: A model of the trajectories and midair collision probabilities of sand particles in a steady state saltation cloud, Journal of Geophysical Research

Atmospheres, 112, 2007.

Huang, N., and Wang, Z. S.: A 3-D simulation of drifting snow in the turbulent boundary layer, Cryosphere Discussions, 9, 301-331, 2015.

Huang, N., Dai, X., and Zhang, J.: The impacts of moisture transport on drifting snow sublimation in the saltation layer, Atmospheric Chemistry & Physics, 16, 7523-7529, 2016.

Huang, N., and Wang, Z. S.: The formation of snow streamers in the turbulent atmosphere boundary layer, Aeolian Research, 23, 1-10, 2016.

Huang, N., and Shi, G.: The significance of vertical moisture diffusion on drifting Snow sublimation near snow surface, Cryosphere, 11, 3011-3021, 2017.

Kok, J. F., Parteli, E. J. R., Michaels, T. I., and Karam, D. B.: The physics of wind-blown sand and dust, Rep Prog Phys, 75, 106901, 10.1088/0034-4885/75/10/106901, 2012.

Lehning, M., Löwe, H., Ryser, M., and Raderschall, N.: Inhomogeneous precipitation distribution and snow transport in steep terrain, Water Resources Research, 44, 278-284, 2008.

Li, D., Wang, Y., Guo, L., and Xiao, F.: Inter-particle collision effects on the entrained particle distribution in aeolian sand transport, International Journal of Heat & Mass Transfer, 58, 97-106, 2013.

Lopes, A., M. G., Oliveira, L., A., Ferreira, Almerindo, D., Pinto, and J., P.: Numerical simulation of sand dune erosion, Environmental Fluid Mechanics, 13, 145-168, 2013.

Lund, T. S., Wu, X., and Squires, K. D.: Generation of Turbulent Inflow Data for Spatially-Developing Boundary Layer Simulations, Journal of Computational Physics, 140, 233-258, 1998.

Mann, G. W., Anderson, P. S., and Mobbs, S. D.: Profile measurements of blowing snow at Halley, Antarctica, Journal of Geophysical Research Atmospheres, 105, 24491-24508, 2000.

Meneveau, C., Lund, T. S., and Cabot, W. H.: A Lagrangian dynamic subgrid-scale model of turbulence, Journal of Fluid Mechanics, 319, 353-385, 1996.

Nemoto, M., and Nishimura, K.: Direct Measurement Of Shear Stress During Snow Saltation, Boundary-Layer Meteorology, 100, 149-170, 2001.

Nemoto, M., and Nishimura, K.: Numerical simulation of snow saltation and suspension in a turbulent boundary layer, Journal of Geophysical Research Atmospheres, 109, D18206, 2004.

Nemoto, M., and Nishimura, K.: Blowing snow at Mizuho station, Antarctica, Philosophical

Transactions of the Royal Society A: Mathematical, Physical and Engineering Sciences, 363, 1647-1662, 10.1098/rsta.2005.1599, 2005.

Nishimura, K., and Hunt, J. C. R.: Saltation and incipient suspension above a flat particle bed below a turbulent boundary layer, Journal of Fluid Mechanics, 417, 77-102, 2000.

Nishimura, K., Yokoyama, C., Ito, Y., Nemoto, M., Naaim‐Bouvet, F., Bellot, H., and Fujita, K.: Snow particle speeds in drifting snow, Journal of Geophysical Research Atmospheres, 119, 9901-9913, 2015.

Okaze, T., Mochida, A., Tominaga, Y., Nemoto, M., Sato, T., Sasaki, Y., and Ichinohe, K.: Wind tunnel investigation of drifting snow development in a boundary layer, Ournal of Wind Engineering & Industrial Aerodynamics, 104-106, 532-539, 2012.

Owen, P.: Saltation of uniform grains in air, Plenum Press, 41, 344-353, 1964.

Raupach, M. R.: Saltation layers, vegetation canopies and roughness lengths, Springer Vienna, 1, 83-96, 1991.

Sørensen, M.: On the rate of aeolian sand transport, Geomorphology, 59, 53-62, https://doi.org/10.1016/j.geomorph.2003.09.005, 2004.

Schneiderbauer, S., and Prokop, A.: The atmospheric snow-transport model: SnowDrift3D, Journal of Glaciology, 57, 526-542, 2011.

Schweizer, J., Jamieson, J. B., and Schneebeli, M.: Snow avalanche formation, Reviews of Geophysics, 41, 1-25, 2003.

Sovilla, B., Burlando, P., and Bartelt, P.: Field experiments and numerical modeling of mass entrainment in snow avalanches, Journal of Geophysical Research, 111, F03007, 2006.

Sugiura, K., Nishimura, K., Maeno, N., and Kimura, T.: Measurements of snow mass flux and transport rate at different particle diameters in drifting snow, Cold Regions Science & Technology, 27, 83-89, 1998.

Sugiura, K., and Maeno, N.: Wind-Tunnel Measurements Of Restitution Coefficients And Ejection Number Of Snow Particles In Drifting Snow: Determination Of Splash Functions, Boundary-Layer Meteorology, 95, 123-143, 2000.

Uematsu, T., Nakata, T., Takeuchi, K., Arisawa, Y., and Kaneda, Y.: Three-dimensional numerical simulation of snowdrift, Cold Reg.sci.technol, 20, 65-73, 1991.

Vinkovic, I., Aguirre, C., Ayrault, M., and Simoëns, S.: Large-eddy Simulation of the Dispersion

514 of Solid Particles in a Turbulent Boundary Layer, Boundary-Layer Meteorology, 121, 283-311,
515 2006.
516 Vionnet, V., Martin, E., Masson, V., Guyomarc'H, G., Naaimbouvet, F., Prokop, A., Durand, Y.,
517 and Lac, C.: Simulation of wind-induced snow transport in alpine terrain using a fully coupled
518 snowpack/atmosphere model, Cryosphere Discussions, 7, 2191-2245, 2013.
519 Walter, B., Horender, S., Voegeli, C., and Lehning, M.: Experimental assessment of Owen's
520 second hypothesis on surface shear stress induced by a fluid during sediment saltation,
521 Geophysical Research Letters, 41, 6298-6305, 2015.
522 Xiao, J., Bintanja, R., Déry, S. J., Mann, G. W., and Taylor, P. A.: An Intercomparison Among
523 Four Models Of Blowing Snow, Boundary-Layer Meteorology, 97, 109-135, 2000.
524 Xue, M., Droegemeier, K. K., Wong, V., Shapiro, A., Brewster, K., Carr, F., Weber, D., Liu, Y., and
525 Wang, D.: The Advanced Regional Prediction System (ARPS) – A multi-scale nonhydrostatic
526 atmospheric simulation and prediction tool. Part II: Model physics and applications, Meteorology
527 & Atmospheric Physics, 76, 143-165, 2001.
528 Yamamoto, Y., Potthoff, M., Tanaka, T., Kajishima, T., and Tsuji, Y.: Large-eddy simulation of
529 turbulent gas-particle flow in a vertical channel: effect of considering inter-particle collisions,
530 Journal of Fluid Mechanics, 442, 303-334, 2001.
531 Zhang, J., and Huang, N.: Simulation of Snow Drift and the Effects of Snow Particles on Wind,
532 Modelling & Simulation in Engineering, 2008, 408075, 2008.
533 Zwaaftink, C. D. G., Diebold, M., Horender, S., Overney, J., Lieberherr, G., Parlange, M. B., and
534 Lehning, M.: Modelling Small-Scale Drifting Snow with a Lagrangian Stochastic Model Based on
535 Large-Eddy Simulations, Boundary-Layer Meteorology, 153, 117-139, 2014.
536

Appendix 1

The aerodynamic entrainment scheme describes the information of fluid entrained particles from the bed surface. According to , the number of entrained particles per unit area per unit time can be written as (Anderson and Haff, 1991):

$$N_{ae} = \eta(\tau - \tau_t) \tag{A1}$$

where $\eta = C/(8\pi d_p^2)$ (Doorschot and Lehning, 2002) and $\tau_t = A^2 g \bar{d}_p (\rho_p - \rho)$ (Clifton et al., 2006), in which $C = 1.5$ and $A = 0.2$ are constants, and $\bar{d}_p$ is the mean diameter of snow particles.

The grain-bed interactions are described by the ejecta number, horizental and vertical restituation coefficients, respectively. The ejecta number n_e follows the binomial distribution (Sugiura and Maeno, 2000):

$$S_e(n_e) = \mathrm{C}_l^{n_e} q^{n_e} (1-q)^{l-n_e} \tag{A2}$$

where q and p are functions of impact velocity v_{in} and incident angle θ_{in}:

$$l = \frac{0.26 v_{in}^{1.2} \theta_{in}^{0.32}}{0.51 v_{in}^{0.6} \theta_{in}^{0.16} - 0.18 v_{in}^{-0.27} \theta_{in}^{0.05}} \tag{A3}$$

$$q = 1 - 0.35 v_{in}^{-0.87} \theta_{in}^{-0.11} \tag{A4}$$

At the same time, the horizontal restitution coefficient e_h and the vertical restitution coefficient e_v can be described by a normal and gamma distribution, respectively:

$$P(e_h) = \frac{1}{\sqrt{2\pi}\sigma} \exp\left(-\frac{(e_h - \mu)^2}{2\sigma^2}\right) \tag{A5}$$

$$P(e_v) = \frac{1}{\beta^\alpha \Gamma(\alpha)} e_v^{\alpha-1} \exp\left(-\frac{e_v}{\beta}\right) \tag{A6}$$

where μ, σ^2, α and β are all expressions of v_{in} and θ_{in}, as shown in Tab. A1.

Parameters	Compact snow	Fresh snow
α	$\begin{cases} 1.22\theta_{in}^{0.47} & v_{in} \geq 0.84\ ms^{-1} \\ 1.22(v_{in}/0.84)^{\log(v_{in}/0.84)}\theta_{in}^{0.47} & 0.84 < v_{in} \leq 1.23\ ms^{-1} \\ 1.22(v_{in}/0.84)^{\log(v_{in}/0.84)}(v_{in}/1.23)^{-2\log(v_{in}/1.23)}\theta_{in}^{0.47} & v_{in} \geq 1.23\ ms^{-1} \end{cases}$	
β	$\begin{cases} 12.85\theta_c^{-1.41} & v_c \geq 0.84\ ms^{-1} \\ 12.85(v_c/0.84)^{-\log(v_c/0.84)}\theta_c^{-1.41} & 0.84 < v_c \leq 1.23\ ms^{-1} \\ 12.85(v_c/0.84)^{-\log(v_c/0.84)}(v_c/1.23)^{\log(v_c/1.23)}\theta_c^{-1.41} & v_c \geq 1.23\ ms^{-1} \end{cases}$	
μ	$\begin{cases} 0.48\theta_i^{0.01} & v_c \leq 1.27\ ms^{-1} \\ 0.48(v_c/1.27)^{-\log(v_c/1.27)}\theta_i^{0.01} & v_c > 1.27\ ms^{-1} \end{cases}$	
σ^2	$\begin{cases} 0.17\theta_c^{-0.25} & v_c \leq 1.27\ ms^{-1} \\ 0.17(v_c/1.27)^{-\log(v_c/1.27)}\theta_c^{-0.25} & v_c > 1.27\ ms^{-1} \end{cases} (u_* = 0.19\ ms^{-1})$ $\begin{cases} 0.08\theta_c^{0.01} & v_c \leq 1.34\ ms^{-1} \\ 0.08(v_c/1.34)^{-\log(v_c/1.34)}\theta_c^{0.01} & v_c > 1.34\ ms^{-1} \end{cases} (u_* = 0.25\ ms^{-1})$	$\begin{cases} 0.07\theta_c^{-0.06} & v_c \leq 0.52\ ms^{-1} \\ 0.07(v_c/0.52)^{-\log(v_c/0.52)}\theta_c^{-0.06} & v_c > 0.52\ ms^{-1} \end{cases}$

Table R1. Parameters of splash function.